Article

Fabrication of a Hydrogenated Amorphous Silicon detector in 3-D geometry and preliminary test on planar prototypes.

Mauro Menichelli[1,*], Marco Bizzarri[1,2], Maurizio Boscardin[3,4], Mirco Caprai[1], Anna Paola Caricato[5], Giuseppe Antonio Pablo Cirrone[6], Michele Crivellari[4], Ilaria Cupparo[7], Giacomo Cuttone[6], Silvain Dunand[8], Livio Fanò[1,2], Omar Hammad[4], Maria Ionica[1],   Keida Kanxheri[1], Matthew Large[10] , Giuseppe Maruccio[5], Annagrazia Monteduro[5], Francesco Moscatelli[1,9], Arianna Morozzi[1], Andrea Papi[1], Daniele Passeri[1,11], Marco Petasecca[10], Silvia Rizzato[5] , Alessandro Rossi[1,2], Andrea Scorzoni[1,11], Leonello Servoli[1], Cinzia Talamonti[7], Giovanni Verzellesi[3,12], Nicolas Wyrsch[8].

1 INFN, Sez. di Perugia, via Pascoli s.n.c. 06123 Perugia (ITALY)
2 Dip. di Fisica e Geologia dell'Università degli Studi di Perugia, via Pascoli s.n.c. 06123 Perugia (ITALY)
3 INFN, TIPFA Via Sommarive 14, 38123 Povo (TN) (ITALY)
4 Fondazione Bruno Kessler, Via Sommarive 18, 38123 Povo (TN) (ITALY)
5   INFN and Dipartimento di Fisica e Matematica dell'Università di Lecce, Via per Arnesano, 73100 Lecce (ITALY)
6   INFN Laboratori Nazionali del Sud, Via S.Sofia   62, 95123 Catania (ITALY)
7   INFN and Dipartimento di Fisica e Astronomia dell'Università di Firenze, Via Sansone 1, 50019 Sesto Fiorentino (FI) (ITALY).
8   Ecole Polytechnique Fédérale de Lausanne (EPFL), Institute of Microengineering (IMT), Rue de la Maladière 71b, 2000 Neuchâtel, (SWITZERLAND).
9   CNR-IOM, via Pascoli s.n.c. 06123 Perugia (ITALY)
10   Centre for Medical Radiation Physics, University of Wollongong, Northfields Ave Wollongong NSW 2522, (AUSTRALIA).
11   Dip. di Ingegneria dell'Università degli studi di Perugia, via G.Duranti 06125 Perugia (ITALY)
12   Dip. di Scienze e Metodi dell'Ingegneria, Università di Modena e Reggio Emilia, Via Amendola 2, 42122 Reggio Emilia (ITALY)
* Correspondence: Mauro.menichelli@pg.infn.it

Abstract:Hydrogenated amorphous silicon (a-Si:H) can be produced by plasma-enhanced chemical vapour deposition (PECVD) of SiH_4 (Silane) mixed with Hydrogen. The resulting material shows outstanding radiation resistance properties and can be deposited on a wide variety of different substrates. These devices have been used to detect many different kinds of radiation namely: MIPs, x-rays, neutrons and ions as well as low energy protons and alphas. However, MIP detection using planar diodes has always been difficult due to the unsatisfactory S/N ratio arising from a combination of high leakage current, high capacitance and a limited charge collection efficiency (50% at best for a 30 μm planar diode). To overcome these limitations the 3D-SiAm collaboration proposes to use a 3D detector geometry.   The use of vertical electrodes allows for a small collection distance to be maintained while conserving a large detector thickness for charge generation. The depletion voltage in this configuration can be kept below 400 V with consequent reduction in the leakage current. In this paper, following a detailed description of the fabrication process, the results of the tests performed on the planar p-i-n structures made with ion implantation of the dopants and with carrier selective contacts will be illustrated.

Keywords: solid-state detectors; position detectors; radiation hard detector; hydrogenated amorphous silicon;   3D detector.

1. Introduction

Hydrogenated amorphous silicon (a-Si:H) is a disordered semiconductor obtained from PECVD (plasma-enhanced chemical vapour deposition) of a mixture of Silane (SiH_4) and Hydrogen at temperatures of 250-300 °C [1]. The resulting material has an irregular arrangement of atoms where not all Si–Si bonds are actually saturated, leading to the presence of dangling bonds (DBs) that are related with the presence of intermediate states between the valence and the conduction bands. The presence of Hydrogen in the mixture has the purpose of passivating most of dangling bonds; in amorphous (non-hydrogenated) silicon (a-Si) the density of defects due to DBs is 10^{19} cm^{-3} while for a-Si:H this density can be as low as 10^{15} cm^{-3}.   The amount of Hydrogen necessary to reach these levels of passivation of the DBs is about 1% atomic, but device grade materials usually exhibit hydrogen concentrations between 4 and 12%. The Hydrogen percentage in the material affects its bandgap (increasing the hydrogen percentage leads to a larger bandgap) and depends on the deposition conditions such as processing temperature. However, temperatures above 350 °C leads to hydrogen desorption, transforming the material into a-Si. This relatively low deposition temperature facilitates the adhesion of a-Si:H on many different substrates like glass (including also pyrex and fused silica), stainless steel, crystalline silicon, silicon oxide, aluminum, coated ceramic, chromium-plated brass, copper-coated PCB, and also organic materials like polyammide, PEN (Polyethylene naphthalate), PET (Polyethylene terephthalate) and PI (Polymide), heat resistant organics/inorganic polymers (like ormocer®) and even on top of electronic devices in CMOS (complementary metal-oxide semiconductor) technology [2]. Usual deposition techniques for detector-quality a-Si:H are: PECVD with plasma excitation at radio frequency (13.56 MHz) [3] or at very high frequencies (between 27 and 150 MHz) [4] or even with microwave frequencies [5]; also hot-wire deposition have been used for the deposition of this material [6].

The relatively wide bandgap of a-Si:H and its disordered nature implies a low charge carrier mobility (1-3 cm^2 V^{-1} s^{-2} for electrons and 0.01 cm^2 V^{-1} s^{-2} for holes) and as a consequence the charge collection time in a 30 µm thick diode is below   15 ns [7]. A-Si:H is a semi-isolating material with a resistivity above 10^{10} Ω cm. This resistivity can be lowered by more than seven orders of magnitude by doping [8]. However, doping of a-Si:H creates additional defects which consequently lowers the carrier lifetime of the material [9]. Therefore, doped layers cannot be employed as active layers in photodiodes or particle sensors. For this reason, p-i-n diode structures, not direct p-n junctions, are preferred with relatively thin p or n doped layers. Usually, this material is doped with the addition of PH_3 (n-type doping) or B_2H_6 or Trimethylboron (p-type doping) in the process gas mixture. It was also demonstrated that similar doping levels and conductivity can be achieved by ion implantation at low temperature [10]. This doping technique was demonstrated by the fabrication of various devices [11,12]. The feature of a-Si:H that makes it attractive for particle detector developments is its remarkable radiation resistance. This has led to significant research activities aiming at single MIP detection [13, 14, 15]. In ref. [16] the radiation tests of a 32.6 µm thick p-i-n diode irradiated at CERN's Proton-Synchrotron with 24 GeV protons up to a maximum fluence of 7×10^{15} p/cm^2 is reported; an increment in leakage current only by a factor of 2 at 9×10^4 V/cm electric field was observed, and this increase disappeared after 24 hours of annealing at 100 °C. Although this material has an extremely high radiation hardness, the main limitation of a-Si:H planar detectors is their poor signal-to-noise ratio for the detection of MIPs that is yet to exceed a value of 5. The reason for this low s/n ratio is the very high depletion voltage (with electric fields up to 10^5 V/cm) that generates a high leakage current (up to about 1 µA/cm^2). Furthermore, the low charge collection efficiency (below 50% for a 30 µm thick diode) due to the disordered nature of the a-Si:H lattice structure contributes to the decrease of the overall value of the signal-to-noise ratio even if some effort has been performed in order to increase charge collection efficiency in these devices [17]. The depletion voltage of an a-Si:H detector V_d is related to the density of DBs (N_{db} number of dangling bonds/volume in cm^3) according to the formula:

$$V_d = \frac{e * N_{db} * d^2}{2\varepsilon}$$

where e is the electron charge and d is the thickness of the depleted layer. If we express d in μm and V_d in Volts we can express this formula as $V_d = k * d^2$, where k ranges from 0.3 to 1.2 when N_{db} ranges from 5×10^{14} to 2×10^{15} cm^{-3}. Furthermore, a large thickness of the detector reduces the charge collection efficiency due to charge trapping over a longer distance.

Increasing the depletion voltage increases the leakage current at full depletion and this increases the noise. To reduce noise and increase the signal we propose to fabricate a p-i-n structured a-Si:H detector in 3D geometry that make possible to keep a relatively small collection distance (namely a 25-35 μm inter-electrode spacing) with a detector thickness up to 100 μm or more, increasing the total charge generated in the detector by a MIP. Having a low distance between the electrodes is important for keeping the leakage current low, reducing the noise. In Figure 1 we show the baseline design for our detector where a-Si:H is deposited over a low resistivity p-type Silicon substrate that distributes the bias to the p-type electrodes on the detector. The n-type electrode collects the signal for the readout electronics connected on the top contacts. This configuration is the basis of developments for Si-3D for High Luminosity (HL) LHC applications. [18]. As seen from a top-down perspective, the electrodes are arranged as shown in Figure 2a where one n-type finger-type electrode is surrounded by 4 p-type finger-type electrodes. Additionally, Figure2 shows alternative electrode configurations: Figure2a is the baseline configuration; Figure2b shows a configuration with 8 p-type finger-type electrodes surrounding an n-type electrode; Figure 2c shows a configuration with 1 finger-type n-type electrode surrounded by 4 trench-type p-type electrodes; and Figure 2d shows alternate all trench-type n and p-type electrodes. Trench electrode configurations have been studied and used for the realization of excellent time resolution silicon detectors, for example in the TIMESPOT collaboration. [19].

As previously stated the main goal that we would like to achieve with this device is an increase in signal-to-noise ratio up to a value of about 10 (without irradiation). Even if a comparison with an equivalent pixel-size, not-irradiated, silicon detector is in favour of c-Si detectors that show typical values in the order of 15-20, after a high dose irradiation the degradation of the signal to noise ratio may favour the more radiation resistant a-Si:H detector. Other relevant quantities like space resolution and track efficiency are strictly related to the signal to noise resolution. In table I some characteristics of a-Si:H versus c-Si are summarized.

The observed relatively small increase of leakage current in a-Si:H versus irradiation fluence makes a-Si:H a possible option for future position and tracking in the increasing fluence trend for future collider experiments.

Table I Summary of c-Si and a-Si:H characteristics

Properties	c-Si	a-Si:H	Remarks
Bandgap (eV)	1.14	1.65-1.8 (for device grade)	For a-Si :H given by Tauc's gap, depends on H content
Density (g/cm3)	2.3290	2.20-2.31 (device grade)	

Hydrogen content (at. %)	0	4-15% (device grade) – 0-50% possible	
e-h creation energy (eV)	3.6	4-6	
e-h creation / μm for MIP	~80 (1)	~80	Stopping power similar (almost same density, effect of H negligible)
e drift mobility (cm^{2}s^{-1}V^{-1})	1450	1-3	
h drift mobility (cm^{2}s^{-1}V^{-1})	450	0.01	
e mobility-lifetime (cm^{2}V^{-1})	~5x10^{-3}	≤5x10^{-5}	For a-Si:H, depends on deposition and treatments
h mobility-lifetime (cm^{2}V^{-1})	~3x10^{-3}	≤10^{-7}	For a-Si:H, depends on deposition and treatments
Full depletion field (V/ μm)	<1	≥10	depends on defect density
Charge collection efficiency	97-99%	40-50% (2)	Depends on charge type, field and time window
Device leakage current not irradiated [A/cm^3]	10^{-3}-10^{-5}	≤10^{-3} (3)	For a-Si:H, thickness and field dependent (a-Si:H bulk, for 10 μm thick diode at field of 10^5 V/cm, non irradiated)
Device leakage current irradiated 5 x 10^{15} p (24 GeV)/cm^2) [A/cm^3]	10^{-1}-10^{-3}	< 3 10^{-3} (4)	For a-Si:H, thickness and field dependent (a-Si:H bulk, for 10 μm thick diode at field of 10^5 V/cm,

(1) Experimentally observed value. Theoretical value is 108 for a stopping value of 1.66 MeV cm^2 g^{-1} for a MIP in c-Si

(2) For transient experiment. Due to deep trapping, holes are in principle not collected. Collection efficiency >80% in steady-state.

(3) Leakage value for planar diode. Diode on non-planar substrates and unpassivated edges can lead to significantly higher leakage.

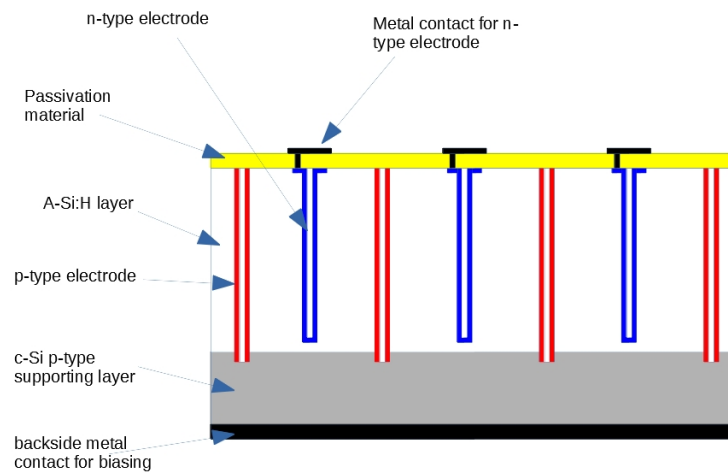(4) Experimental value not available. Increase of leakage by 2-3 for 32 μm thick diodes.

Figure 1 Baseline configuration of a a-Si:H detector. P-type electrodes take the bias voltage from the p-doped c-Si substrate while n-type electrodes are connected to the readout electronics
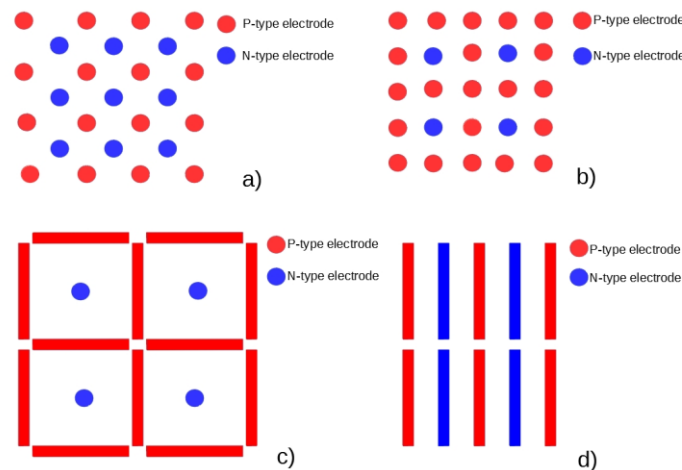

Figure 2 3D a-Si:H detectors configurations: a) finger-type n-doped electrode surrounded by 4 finger-type p-doped electrodes. b) finger-type n-doped electrode surrounded by 8 finger-type p-doped electrodes. c) finger-type n-doped electrode surrounded by 4 trench-type p-doped electrodes. d) all trenches configuration.

2. The fabrication of a 3D detector

The fabrication of a 3D detector in a-Si:H is somewhat different from the construction of a 3D detector in crystalline silicon due to the constraint of keeping the temperature of processing below 250-300 °C in order to avoid hydrogen desorption.

The process starts with the deposition on support wafers (typical a Cz low resistivity p-type silicon wafer with a resistivity below 10 Ωcm) of the a-Si:H performed via PECVD with a VHF excited plasma at the frequency of 70 MHz. The plasma is composed by a

mixture of silane and hydrogen (ratio of 1 to 1) at temperatures around 200°C and will produce a layer with thickness of around 100 μm.

After that, both the ohmic and junction columns will be defined and etched using a Deep Reactive Ion Etching (DRIE) apparatus based on Bosh process. This technique allows the etching of a hole with a diameter of few microns and with a high aspect ratio (more than 50). The ohmic columns will be deeper than the a-Si:H layer (partially etching the c-Si substrate)   meanwhile the junction columns will be about 20 μm less deep than a-Si:H thickness.

Afterwards the etched holes in the a-Si:H layer must be doped in the internal surfaces. In order to create the p-i-n structure in the detector, two separate masks will be fabricated to define an n-plus region and a p-plus region. Doping the detector inside the holes cannot be performed using commonly employed techniques for planar structures (i.e. PECVD deposition of doped a-Si:H) as these deposition techniques cannot achieve the required conformality on deep trenches [20,21]. Therefore, two doping options will be considered:

- **Option 1:** Atomic Layer Deposition (ALD) of conductive metallic oxides for the creation of   selective contacts for each type of charge carriers: titanium oxide for electron selective contact and tungsten or molybdenum oxide for hole selective contacts. Since the oxides for charge selective contacts are quite resistive, it is   foreseen to deposit a conductive metal inside the holes or trenches by PLD (Pulsed Laser Deposition).
- **Option 2:** Ion implantation of boron (p-type doping) and phosphorous (n-type doping) followed by a temperature activation annealing process below 200°C or an additional metal deposition by PLD if needed.

In order to have a reasonable time constant (order of 10 ns) for charge collection the resistance of the electrodes should be in the order 1 Mohm.

After the doping, a contact hole will be open and the metal (typical Al 1% Silicon) will be deposited and defined. The passivation, based on a multilayer of Si_3N_4 and SiO_2, will be deposited by low-temperature PECVD technique and subsequently opened to allow the contact of the metal layer. The final step is the metal deposition of the backside that will be used as bulk bias contact.
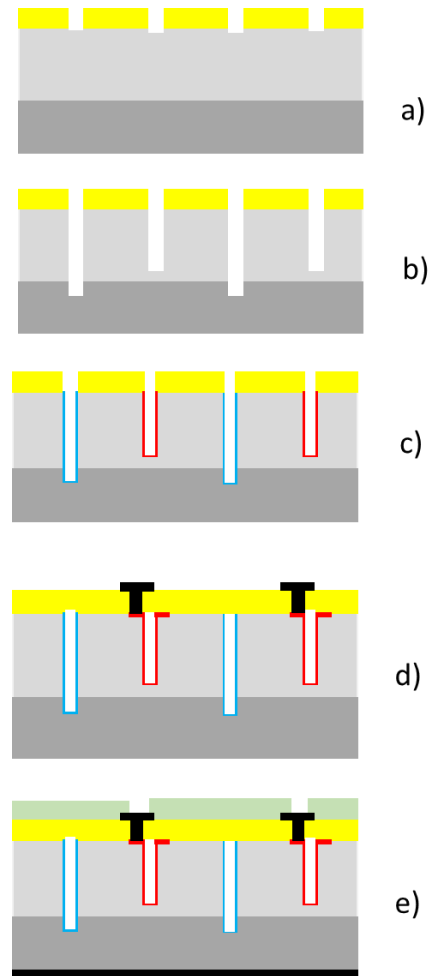
Figure 3 Process description of 3D a-Si:H detector fabrication (option 2), lithographic steps are omitted. a) Silicon Nitride passivation layer deposition and patterning for DRIE process. b) p-hole and n-hole etching   c) Columns doping by ion implantations . d) Opening of contacts, metal deposition and etching. e) deposition and patterning of passivation layer. and deposition of backside metal.

3. Results on phase I prototype.

Most of the technological challenges foreseen for the fabrication a 3D detector built on a-Si:H needs to be addressed by the construction of prototypes especially devoted to these purposes. A first phase of prototype production should mainly verify if the two doping options, mentioned in the previous chapter, can actually produce efficient junctions for biasing the intrinsic layer and to create an effective charge collection in the construction of a diode that can actually generate rectification properties. A second generation of prototypes (presently under design) should be able to measure the relation between etching rate and hole diameter in the DRIE process on a-Si:H. Since p type electrodes should go deep enough in the a-Si:H layer to erase a shallow layer of substrate while n-type electrode should be fully contained in the a-Si:H layer, we would like to verify the possibility of etching p and n type electrodes in one single process exploiting the fact that larger diameter holes have a faster etching rate compared to narrower holes.

3.1. Leakage current test on option 1

Concerning option 1 related to the use of selective contacts, vertical structures have been fabricated on chromium-plated glass substrates. As electron selective contacts, ZnO:Al (Aluminum doped Zinc Oxide AZO) and TiO_2 (respectively 60 nm and 10 nm thick) layers have been implemented on the substrate side and compared. As a hole selective contact, MoO_x (20 nm thick) protected by an Indium Thin Oxide layer (60 nm) has been deposited. All selective contacts have been deposited by sputtering for convenience. Note that for 3D architecture, ALD should be used to enable conformal deposition in the holes or trenches. First I/V results for 2 diodes are given on Figure4 for vertical diodes with an area of 0.25 cm². From the figure we can observe   that a good rectifying behavior can be observed (almost 3 orders of magnitude for AZO and 2 orders of magnitude for TiO_2). The leakage current is about 4 nA/cm² comparable with the samples obtained with ion implantation doping. For these promising results this doping technique can be considered as a good alternative to implantation and it will be studied further.
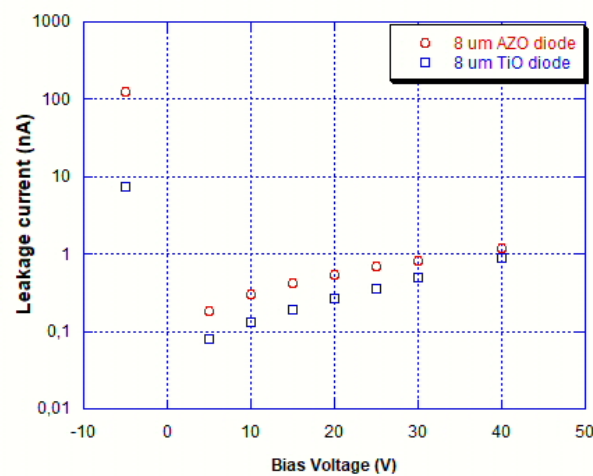

Figure 4. Leakage current vs. bias field for 2 vertical detectors with charge selective contacts with having 8 μm thickness biased up to 5V/ μm electric field: a sample is fabricated using TiO_2 electrons selective contact and the other sample is fabricated using ZnO:Al (AZO) electron selective contact. MoO_x/ITO are used in both devices as hole selective contact.

3.2. Leakage current tests on doping option 2.

In order to verify the feasibility of doping intrinsic a-Si:H inside the holes fabricated via the DRIE process to build effective 3D   p and n type electrodes,   the two doping options explained in the previous chapter have been verified with the construction of two types of prototypes: vertical diodes and lateral diodes in a planar configuration obtained from the deposition of a layer of 10 μm of a-Si:H on a heavily doped p-type c-Si substrate (300 μm thickness).

Vertical diodes, shown in figure5, use the p-type c-Si silicon substrate as the p-type biasing electrode and the n-type electrode is obtained via ion implantation of Phosphor ions. Diodes with several geometries have been produced, namely single diodes, 2 x 3 diodes arrays, 2 x 10 diodes array and strip detectors.
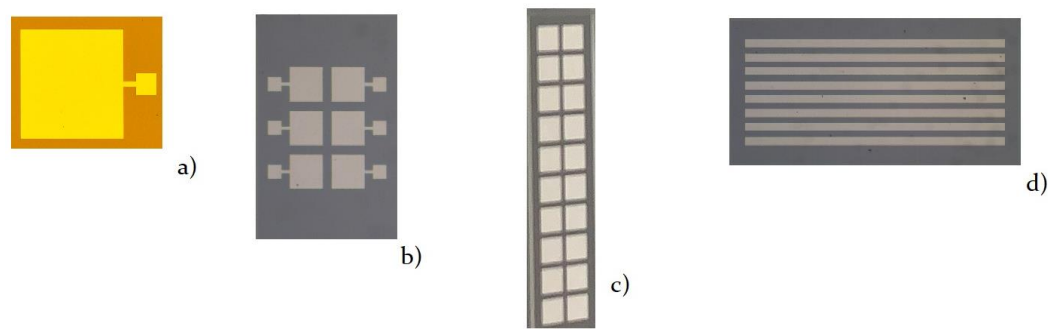
Figure 5. Vertical diodes configurations a) Single diode 1.25 x 1.25 mm² . b) 2 x 3 diode array c) 2 x 10 diode array d) 8 strip device.

Figure 5 shows an I/V test on two samples of a 4 mm² vertical diode. As shown in the figure, the diode acts as a rectifying junction and the leakage current with 50V bias is about 147 pA with a current density of 3.6 nA/cm² on the best sample.
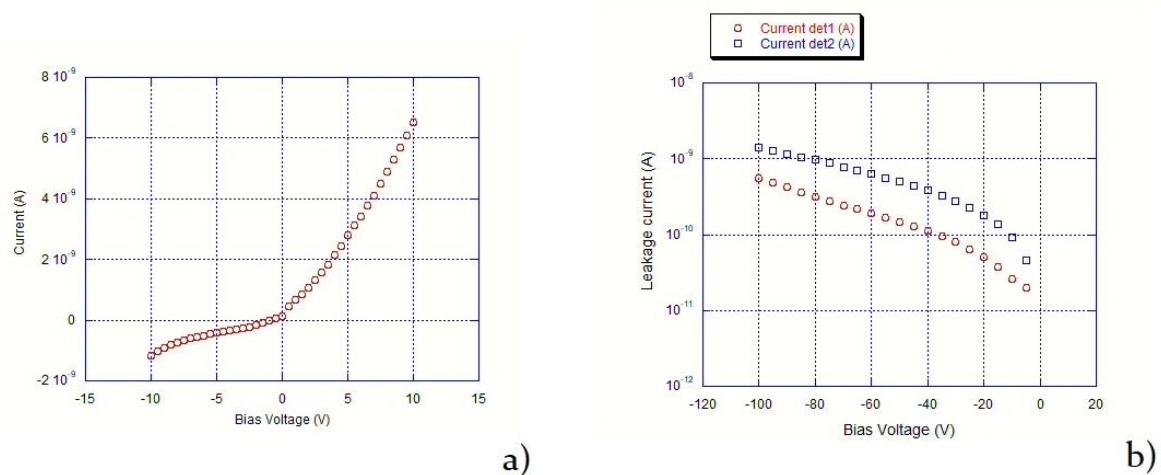

Figure 6 a) I/V plot on a vertical 4 mm² diode where the rectifying behavior is evident. b) reverse current versus bias voltage on two detector samples at 50V leakage currents are: 147 and 496 pA for det 1 and det 2 respectively corresponding to current densities of 3.6 and 12.4 nA/cm² .

Lateral diodes, shown in figure 7 in various configurations, are made with the two electrodes on the same side of the a-Si:H deposition in various geometries with the sensitive part laying between the p- and the n-type electrode both implanted with, respectively: Boron and Phosphorous. In this case, between the a-Si:H layer and the silicon substrate, a thin (500 nm) layer of Silicon oxide has been deposited.

The I/V test (figure 8) shows an even more pronounced rectifying behavior on lateral diodes compared to vertical diodes. In this case leakage current is very low ranging from 339 pA (best small detector) to 1030 pA (worst large detector).

Figure 7. Lateral diode configurations: a) strip detector. b) Comb and Strip detectors the comb is p-doped while the strips are n-doped. c) double comb detector. d) circular device the central electrode is n-doped while the external electrode is p-type. e) 3 x 3 array of circular detectors.
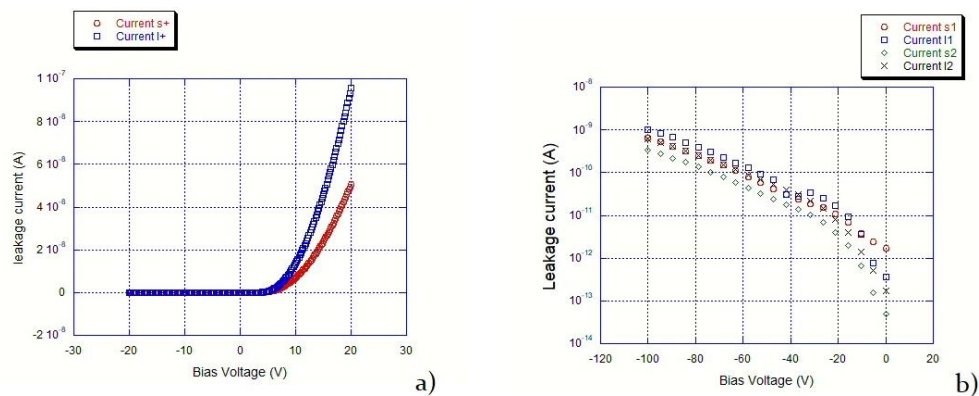

Figure 8. Leakage current vs. Bias voltage in lateral detectors: a) direct and reverse biasing. b) reverse bias only

4. Testing with x-ray

Since this devices are too thin for MIP signal detection we tested the radiation detection capabilities of these diodes using x-rays. Figures 9a and 9b show the linearity of the response of devices with different thickness of the substrate and two different areas of the junction. The sensors are irradiated by a 6MV medical linear accelerator in standard conditions (source to surface distance of 100 cm, field size of 10x10 cm^2 and an equivalent water depth in a plastic phantom of 1.5 cm). Despite the sensors being configured in photovoltaic mode and the high degree of disorder of the substrate material, the adopted configuration of a doped area above an intrinsic amorphous layer allows for the collection of the charge in proportion to the thickness substrate and the area of the sensor as expected.

In Addition, the timing response of the sample with 10um thick substrate and an area of 5x5 mm^2 (Figure9,c) shows a stable response during the irradiation (beam-ON) within 2.2%, well within the expected fluctuations of the machine output [22].

Additional measurement has been taken in order to determine the stabilization time after turn on and the linearity of x-ray flux measurements. Concerning the turn-on stabilization time of the leakage current in the detector we report in Figure10 a measurement of dark current versus time after turn-on on a vertical diode having 10μm thickness 2 x 2 mm^2 area with 25 V bias. Figure 10a shows the measurement on a 2700 s time scale after turn on and figure 10b shows the same data on a 200 s time scale. These results shows that the measurement of dark current became stable after about 200-250s and after that time the current fluctuations are in the order of 80 pA.
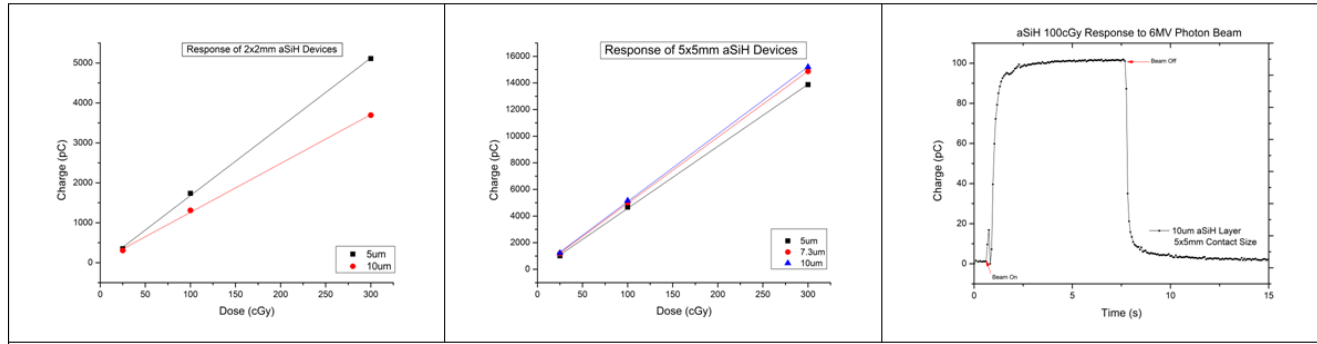
Figure 9:a) Response of pad sensors with different thicknesses to 6MV photon irradiation; a) area of the sensor 2x2 mm²; b) area of the sensor 5x5 mm²; c) timing response of a 5x5mm², 10um thick sensor.
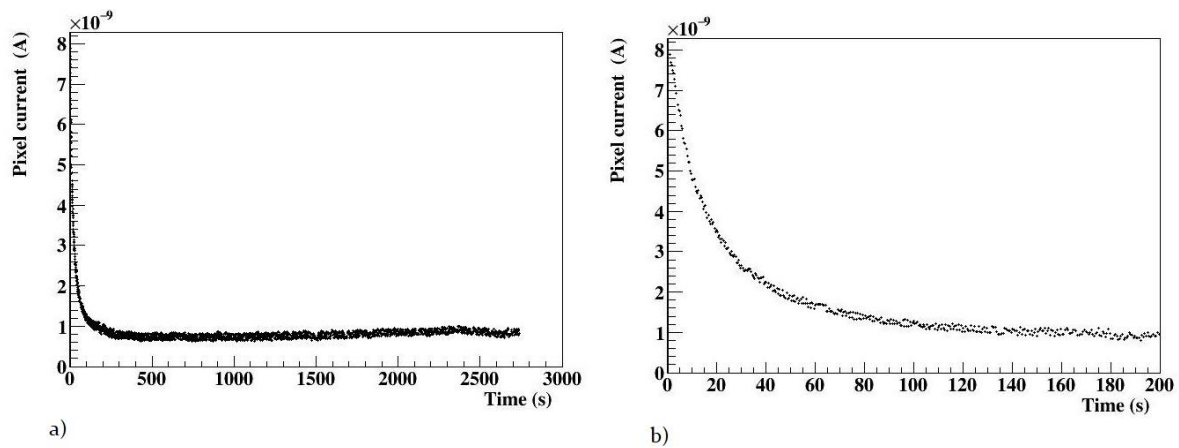

Figure 10 a) leakage current versus time in a 2700 s   time scale. b) leakage current versus time in a 200 s   time scale
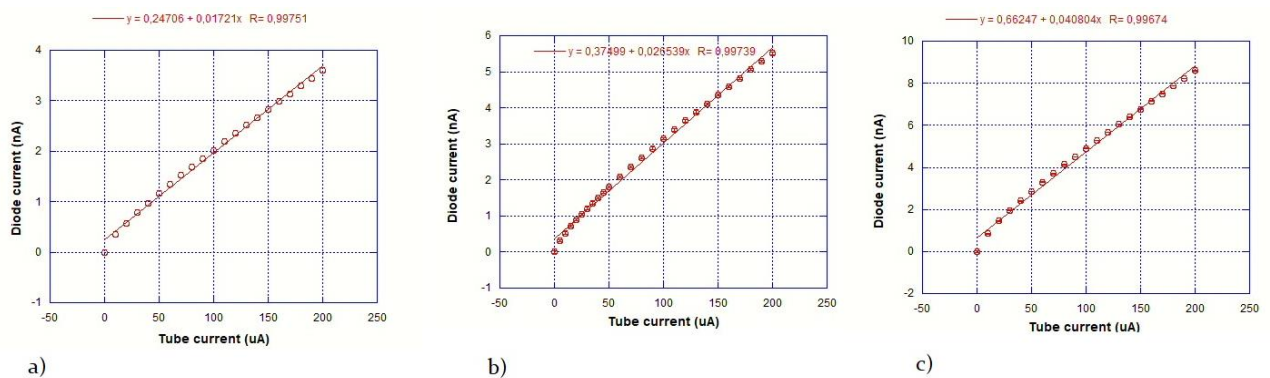

Figure 11 a) Diode current versus X-ray tube current with diode biased at 25V, b) Diode current versus X-ray tube current with diode biased at 50V, c)   Diode current versus X-ray tube current with diode biased at 100 V.

Using the same device we measured the linearity of response to x-ray fluxes using a x-ray tube with tungsten cathode   biased at 10 kV. Figure 11 shows the diode current response (after dark current subtraction)   to irradiation at various tube currents for diode bias at 25V (Figure 11a), 50V (Figure 11b) and 100V (Figure 11c), we notice that the linearity is quite good in all cases in the current range between 0 to 200 µA it improves a lot if we consider fluxes above 30 µA.

5. TCAD simulation of a full 3D detector

Different geometrical configurations are being studied by means of device level simulator Synopsys Sentaurus TCAD [23]. A proper description of the a-Si:H material has been included within the material library of Sentaurus TCAD [24]. In particular, full column electrodes, hybrid trench/column electrodes (Mini Trenches) and full trench electrodes have been considered (Figure12). For sake of computational effort, a 3D slice of the whole device depth has been considered, looking at the electric field map distributions (steady-state simulations) and at the current vs. time response to a particle hit (transient simulation) of the different configurations.
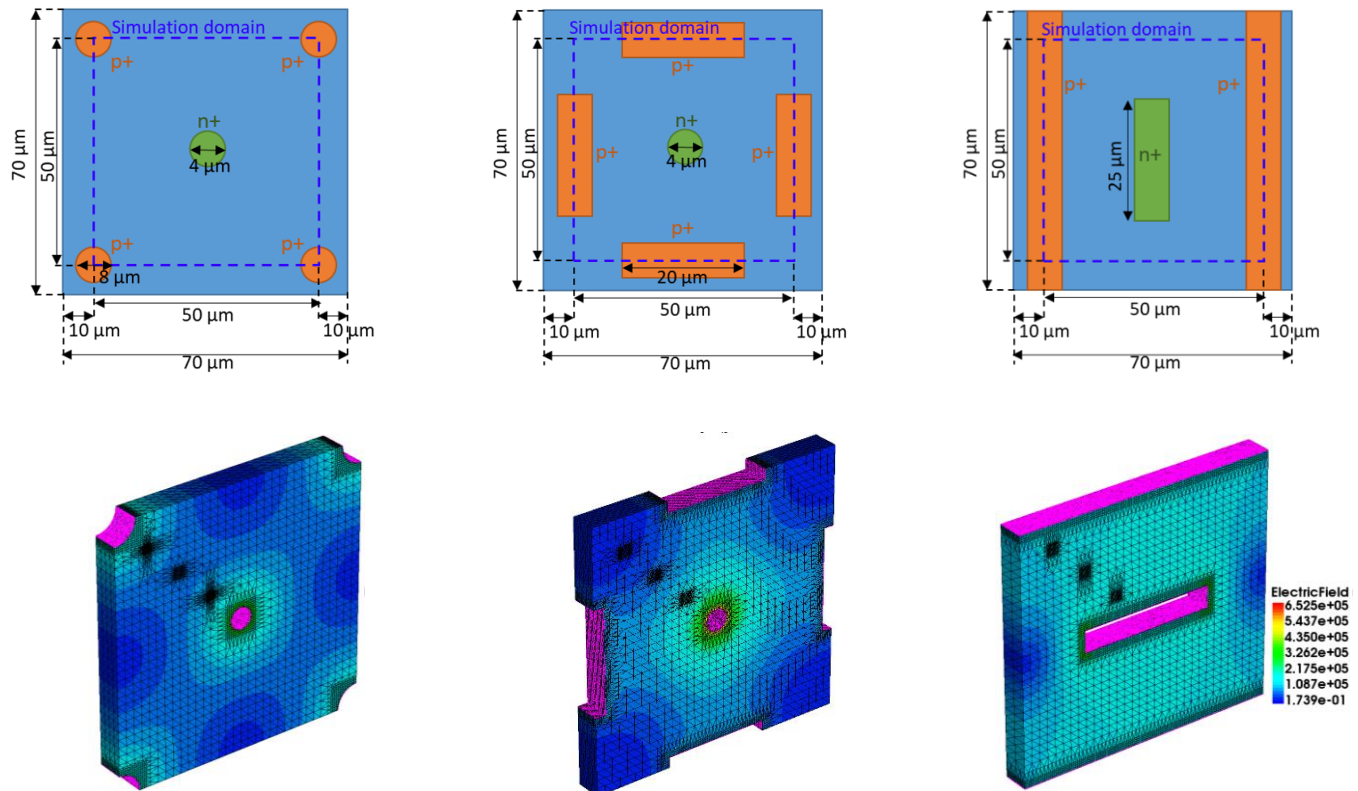

Figure 12 Simulated cells for the different 3D electrodes configurations, from left to right: (a) full columns, (b) hybrid trenches/columns, (c) full trenches.

Depending on the electric field distribution at the particle hit position, different amplitude and timing characteristics of the current response of the device can be appreciated. A faster and higher-current response can be seen with trenches configurations (full lines in Figure 13) with respect to full columns configuration (small dashed lines in Figure13), in particular for particle hits close to the read-out electrode (blue and green curves in Figure13). All currents in the graph are calculated for a 300 V bias.

By integrating the time responses at the read-out electrode, the charge collection properties of the different configurations at different biasing conditions can be evaluated. This study will enable the choice of the optimal, yet technology compatible, detector configuration.
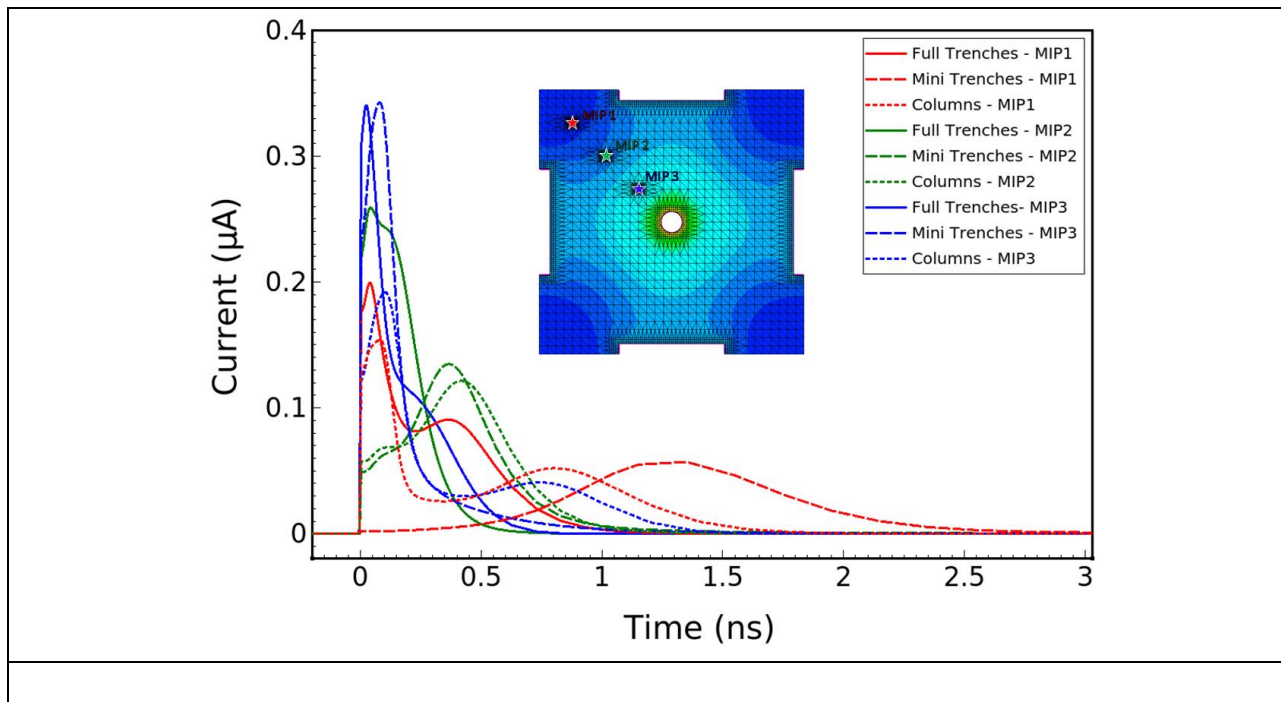
Figure 13 Current pulse generated by a MIP hit in various points in the various configurations. Solid curves refers to the full trench configuration, small dashes is for the all columns configuration and large dashes refers to the mixed columns-trench configurations, colors are related to the hit position as shown in the superposed image for the mixed configuration.

6. Conclusions and outlook

The fabrication of a 3D a-Si:H particle detector as detailed in this paper presents a new detector technology based on the peculiar properties of this material. A preliminary description of this fabrication process has already been given in another paper [25]. The fabrication process has been described here in detail and the R & D process towards the clarification of the feasibility of the detectors has been explained. The early results of the first generation of prototypes have been presented demonstrating the capability of producing a working planar p-i-n diode with a quite low leakage current. We consider the first phase of prototype development as satisfactory and have begun the second phase.

Detectors will be also tested after fabrication with radioactive sources like ⁹⁰Sr, electron accelerators and collimated x-ray sources. After this, preliminary test detectors will be irradiated with proton, neutron and gamma-rays from a Cobalt-60 source for the evaluation of displacement and ionization damage. A new test run with the above-mentioned sources is then foreseen.

In order to obtain charge collection efficiency maps of charge particle interacting with the detector, a test at the Australian Nuclear and Science Technology Organization (ANSTO – Lucas Heights – NSW, AUSTRALIA) Ion Beam Induced Charge facility (IBIC) is also foreseen. The IBIC technique will be used to measure the charge collection efficiency of the 3D device under test (DUT) using a ~1 μm spot size focused ion beam scanning the DUT surface. The response of the DUT stimulated by the particle are correlated with the position of the beam allowing to create a map of the efficiency of the device [26,27]. The IBIC measurements will be performed using the heavy ion microprobe upon the ANTARES 10MV Tandem Accelerator. Various sources are available including the 5.5 MeV helium ion beam having a range of 28 μm in silicon which has been already used successfully in previous works [28].

The device will be also evaluated as a dosimeter using x-ray beams for imaging (kV energy range) and therapeutic applications (MV energy range). The presence of two

doping species allows for the use of these devices in photovoltaic mode (with no bias applied across the contacts). This property is particularly important for dosimetry where a continuous current is readout from the device and dark currents limit the minimum threshold of detectable dose delivered. The test structures fabricated within the 3D-SiAm collaboration have been tested to verify if the quality of the substrate and implantation guarantee the response sensitivity and reproducibility required by the most recent Code of Practice for dosimetric measurements [29] in MV photon radiation fields.

The wide range of materials on which a-Si:H can be deposited on, opens the possibility of the direct deposition of the detector material directly onto the readout chip. This feature has been already exploited in the past [2]. This detector technology called TFA (Thin Film on ASIC) gave the best results in terms of Signal-to-Noise ratio in a planar a-Si:H detector for MIPs detection (S/N ratio of 5 for a MIP). The deposition of a planar detector on present technology front end chip may increase this Signal-to-Noise ratio to higher values. Furthermore, a new technological frontier for the future can be the direct deposition of a 3D a-Si:H detector directly on the readout chip. The usage of DRIE technology for the fabrication of electrode with two different lengths and the selective implantation on different finger type electrodes will allow the fabrication of a detector like the one shown in Figure14, where the n-type electrode reach the readout pad of the readout chip and the p-type electrode do not reach the readout chip. After ion implantation, a passivation and a metallization layer to distribute the biasing contacts to the p-type electrodes will be added.
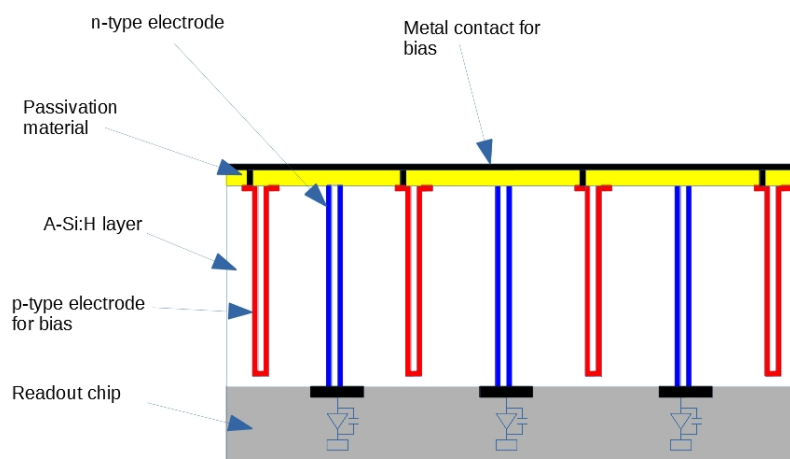

Figure 14 3D a-Si:H detector deposited on a readout chip. N-type electrodes are connected directly on the readout pad of the chip while p-type electrodes are connected to a common biasing plane.

7. Patents

A-Si:H 3D detector is patented in Italy (Patent number N. 102018000010735) and it is patent pending in Europe (Application number EP19831899.0)   and in the U.S. (Application number 17297441).

Author Contributions: "Conceptualization, coordination and editing M.Menichelli, Nanofabrication N. Wyrsch, S. Dunand, M.Boscardin, M.Crivellari, G.Verzellesi, A.P.Caricato, G.Maruccio, A.Monteduro, G.Quarta, and S.Rizzato; I/V testing, F.Moscatelli, A.Rossi, L.Fanò, O.Hammad; x-ray testing and dosimetry L.Servoli, K. Kanxheri, G.Rossi, M. Petasecca, M.Large, G.A.P. Cirrone, G.Cuttone, I. Cupparo, C.Talamonti Test setups M. Bizzarri, M.Caprai, M.Ionica, A.Papi; Simulations D. Passeri, A.Scorzoni, A.Morozzi, M.Petasecca. M.Large   All authors have read and agreed to the published version of the manuscript."

Conflicts of Interest: The authors declare no conflict of interest

References

[1] N. Wyrsch, C. Ballif. Review of amorphous silicon based particle detectors: the quest for single particle detection. *Semiconductor Science and Technology 31 103005 (2016).*

[2] M. Despeisse et al. Hydrogenated amorphous silicon sensor deposited on integrated circuit for radiation detection. *IEEE Trans. in Nucl. Scie. Vol 55. N.2 802-811 (2008).*

[3] B. Rech, et al. Material basis of highly stable a-Si:H solar cells *Mater. Res.Soc. Symp. Proc. 420 33 (1966)*.

[4] S. Shah, J. Dutta, N. Wyrsch, et al. VHF plasma deposition: a comparative study *Mater. Res. Soc. Proc. 258 15–26 (1992)*.

[5] L. Paquin et al. Amorphous silicon for photovoltaics produced by new microwave plasma-deposition techniques. *Can. J. Phys. 63, 831–7 (1985)*.

[6] A. Mahan. Hot wire chemical vapor deposition of Si containing materials for solar cells. *Sol. Energy Mater. Sol. Cells 718 299–327 (2003)*.

[7] M. Despeisse et al. Characterization of 13 and 30 μm thick hydrogenated amorphous silicon diodes deposited over CMOS integrated circuits for particle detection application. *Nucl. Instr. and Meth. A 518 357–361(2004)*

[8] W. E. Spear and P.G. Lecomber. Electronic properties of substitutionally doped amorphous. Si and Ge. *Phil. Mag. 33 935–49. (1976)*.

[9] R. A. Street. Doping and the fermi energy in amorphous silicon *Phys. Rev. Lett. 49 1187–90 (1982)*.

[10] W. E. Spear and P.G. Lecomber. Electrical and photoconductive properties of ion implanted amorphous silicon, *J. of Non-Cryst. Sol. 35-36 pp. 327-332 (1980).*

[11] F. J. Demond, G. Muller, S. Kalbizer, W. E. Spear   and P.G. Lecomber. Hydrogen in gas phase and ion implantation doped amorphous silicon. *Nucl. Instr. and Meth. A, 191 59-62 (1981).*

[12] T. Chikamura, Y. Aoki, K. Yano, T. Komeda, T. Ishihara, Spectral response of boron-implanted amorphous silicon Schottky diode, J. of Appl. Phys. 57 2280 (1985). N. Wyrsch et al. Radiation hardness of amorphous silicon particle sensors. *J. Non-Cryst. Solids 352 1797–800 (2006).*

[13] Pochet T., Dubeau J., Equer B., Karar A., Hamel L. A.   High reverse voltage amorphous silicon p-i-n diodes *J. of Appl. Phys. 68 1340-1344 (1990)*

[14] Fujieda I. *et al.*   Field Profile Tailoring in a-Si:H Radiation Detectors *Mat. Res. Soc. Symp. Proc. 192 399-404 (1990).*

[15] Perez-Mendez V. *et al.* Amorphous Silicon Based Radiation Detectors *J. of Non-Cryst. Sol. 137-138 1291-1296 (1991)*

[16] N. Wyrsch et al. Radiation hardness of amorphous silicon particle sensors. *J. Non-Cryst. Solids 352 1797–800 (2006).*

[17] I Fujieda et al. Improved charge collection of the buried p-i-n a-Si:H radiation detectors. *IEEE Trans. On Nucl. Scie. Vol. 37, N.2, 124-128 (1990)*

[18] G.-F. Dalla Betta, M. Boscardin, G. Darbo, R. Mendicino, M. Meschini, A. Messineo, S. Ronchin, D.M.S. Sultan, N. Zorzi Development of a new generation of 3D pixel sensors for HL-LHC. *Nucl. Instr. And Meth. A   824, 386 – 387 (2016).*

[19] G.T. Forcolin, R. Mendicino, M. Boscardin, A. Lai, A. Loi , S. Ronchin , S. Vecchi and G.-F. Dalla Betta, Development of 3D trenched-electrode pixel sensors with improved timing performance.   *JINST 14 C07011 (2019).*

[20] C. C. Tsai. J. C. Knights. G. Chang, B Wacker, Film formation mechanisms in the plasma deposition of hydrogenated amorphous silicon, *J. Appl. Phys. 59, 2996-3001 (1986).*

[21] Ching-Mei Hsu et al. High-Efficiency Amorphous Silicon Solar Cell on a Periodic Nanocone Back Reflector, *Adv. Energy Mater. 2, 628–633 (2012).*

[22] R. Ravichandran et al. Evaluation methods for detecting changes in beam output and energy in radiation beams from high-energy linear accelerators, *J Med Phys. 32(3): 92–96 (2007).*

[23] TCAD - Technology Computer Aided Design (TCAD) | Synopsys

[24] J. A. Davis et al. Modeling a Thick Hydrogenated Amorphous Silicon Substrate for Ionizing Radiation Detectors. *Frontiers in Physics 2020 Vol. 8,   158.*

[25] M. Menichelli et al.   3D Detectors on Hydrogenated Amorphous Silicon for particle tracking in high radiation environment. *J. Phys.: Conf. Ser. 1561 012016 (2020).*

[26] R. Siegele, D. D. Cohen, and N. Dytlewski. The ANSTO high energy heavy ion microprobe. *Nucl. Instr. And Meth. B 158, 31-38, (1999).*

[27] J. F. Ziegler, M. D. Ziegler, and J. P. Biersack, SRIM–The stopping and range of ions in matter,   *Nucl. Instr. and Meth. B 268, 1818-1823, (2010).*

[28] Sultan F. Alhujaili   et al. Characterization of an "Edgeless" Dosimeter for Angular Independent Measurements in Advanced Radiotherapy Treatments, *IEEE Transactions on Radiation and Plasma Medical Sciences Volume: 3 , Issue: 5 , 579-587 (2019).*

[29] IAEA TRS483 International Atomic Energy Agency (IAEA) 2017, Vienna.